International Journal of Thermophysics, Vol. 27, No. 3, May 2006 (© 2006)
DOI: 10.1007/s10765-006-0064-z

A Study on Thermal Contact Resistance at the Interface of Two Solids

X. Zhang,[1,2] P. Z. Cong,[3] and M. Fujii[1]

Received July 8, 2005

In this paper, numerical simulations and measurements of the thermal contact conductance (TCC) at the interface between the plane ends of two cylinders in contact are carried out. The random model of surface roughness is developed, and the non-dimensional basic equations are solved based on a grid system with equi-peripheral intervals in the azimuthal direction that can express reasonably the real contact spot distribution. The effects of the contact pressure, the thermal conductivity of the interstitial medium, and the mean absolute slope of the rough surface on the TCC were clarified by using a network method. In the experiments, four pairs of brass cylinders, each of which has similar surface topology, are used for the TCC measurements. The hysteretic nature of TCC versus contact pressure was observed in the first loading cycle. The present numerical results show that the TCC increases linearly with the mean absolute slope of the surfaces even at the same mean roughness. Such a tendency agrees well with the measurements.

KEY WORDS: equi-peripheral grid; numerical simulation; thermal contact conductance; thermal contact resistance.

1. INTRODUCTION

The thermal contact resistance (TCR) or thermal contact conductance (TCC = 1/TCR) at the interface of two solids in contact plays an important role in many engineering applications such as the cooling of electronic devices [1]. Although a large number of studies [2–8] since the 1950 s have

[1] Institute for Materials Chemistry and Engineering, Kyushu University, Kasuga 816-8580, Japan.
[2] To whom correspondence should be addressed. E-mail: xzhang@cm.kyushu-u.ac.jp
[3] Interdisciplinary Graduate School of Engineering Sciences, Kyushu University, Kasuga 816-8580, Japan.

been carried out to clarify the effects of the surface topography, that is, the surface roughness and mean surface absolute slope on TCR, the existing analytical models are applicable only to limiting cases [9] and it is still difficult to establish a general expression that can predict accurately the TCR in practical engineering applications. The reasons are mainly due to the difficulties to characterize the actual surface topology quantitatively and accurately. The measurement of the mean surface slope, for example, largely depends on the resolution of the roughness measurement instrument. To overcome these difficulties, Tomimura et al. [10] and Zhang et al. [11] developed a new surface roughness model based on the superposition of sine waves with random parameters. The roughness model has been proved to be valid and can be used effectively in numerical simulations through comparison with the corresponding experimental results.

In this paper, detailed numerical simulations of thermal contact conductance were carried out for various surface configurations and contact pressures, where the basic equations and boundary conditions were dimensionless based on the mean surface roughness. A grid system with equiperipheral intervals in the azimuthal direction was developed to express reasonably the real contact spot distribution, and a network method based on this grid system was used to calculate the TCC. The effects of the contact pressure, the thermal conductivity of the interstitial medium, and the mean surface absolute slope on TCC were investigated. Further, the TCC of the four pairs of brass cylinders in contact at the plane ends was measured. The actual surface roughness of all test cylinders was measured and analyzed, and four combinations of test cylinders with similar surface topology were chosen. The hysteretic nature of the pressure on the TCC was observed in the first loading cycle. The present numerical results agree well with those of the corresponding experiments.

2. NUMERICAL SIMULATIONS

2.1. Physical Model in Simulations

Figure 1 shows the physical model and coordinate system for the simulations of heat conduction through the interfaces. A pair of specimens of length L and diameter d is pressed together with an equivalent mean contact pressure P_m. Specimens I and II have thermal conductivities, k_I and k_{II}, and maximum roughness heights, $R_{max\,I}$ and $R_{max\,II}$, respectively. A uniform heat flux, q_m, is assumed at the bottom surface of the lower specimen ($z=0$), a uniform temperature, T_c, is assumed at the top surface of the upper specimen ($z=2L$), and the side surface of the two specimens ($r=D/2$) is thermally insulated.

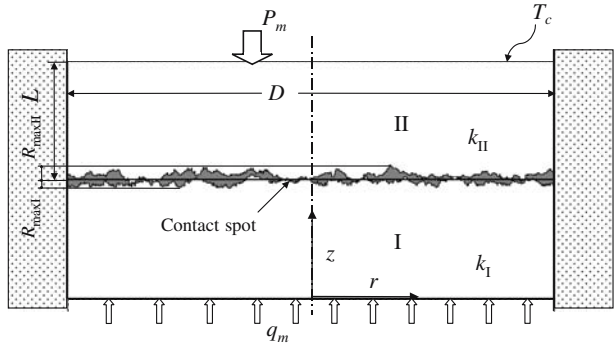

Fig. 1. Physical model for simulations of heat conduction through the interfaces.

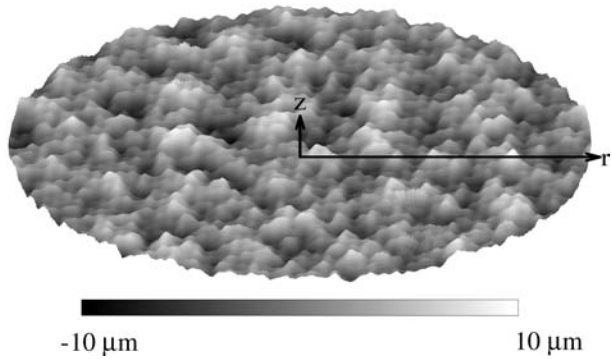

Fig. 2. Simulated result of surface roughness in cylindrical coordinates using random numbers model ($Ra = 2.2\,\mu$m, $l_{min} = 2 \times 10^{-4}$ m, $l_{max} = 2 \times 10^{-2}$ m).

2.2. Non-Dimensional Surface Roughness Model

The present surface roughness model in dimensional form was already described in Ref. 11. A typical rough surface constructed with some average roughness and minimum and maximum wavelengths is shown in Fig. 2. This model is confirmed to have a self-affinity and exhibit a height distribution close to a 'normal' or Gaussian probability distribution.

In this paper the model is non-dimensionalized based on the average surface roughness, Ra, as follows:

$$Z(R,\theta) = B \sum_{i=1}^{n} \sin\left[\frac{2\pi R \cos(\theta + \alpha_i)}{L_i} - \varphi_i\right] \tag{1}$$

$$R = \frac{r}{Ra}, \quad L_i = \frac{l_i}{Ra},$$
$$B = \frac{1}{\frac{1}{\pi R_o^2}\int_0^{2\pi}\int_0^{R_o}\left|\sum_{i=1}^{n}\sin\left[\frac{2\pi R\cos(\theta+\alpha_i)}{L_i}-\varphi_i\right]\right| R\mathrm{d}R\mathrm{d}\theta} \tag{2}$$

where r and R are the dimensional and non-dimensional radii, θ is the angle, R_o is the dimensionless outer radius of the specimen, n is the number of superposed sine waves used to construct a rough surface, l_i and L_i are the dimensional and non-dimensional wavelengths, and φ_i and α_i are the initial phase and orientation of i-th waves. The parameters, L_i, φ_i, and α_i, are expressed randomly by the following equations:

$$\begin{aligned} L_i &= (L_{\max} - L_{\min})\, RND_{i,1} + L_{\min} \\ \varphi_i &= 2\pi\, RND_{i,2} \\ \alpha_i &= 2\pi\, RND_{i,3} \end{aligned} \tag{3}$$

Here $RND_{i,1}$, $RND_{i,2}$, and $RND_{i,3}$ are the random numbers and $L_{\min}$ and $L_{\max}$ are the minimum and maximum dimensionless wavelengths, respectively. This model can reproduce the actual surface roughness having an arbitrary height distribution and mean slope of roughness by choosing the dimensionless parameters $L_{\max}$, $L_{\min}$, α_i, and φ_i. It is noted that the mean surface roughness does not appear explicitly.

To analyze the effects of various parameters on the TCC, the dimensionless temperature, Θ, the pressure, P, the thermal conductivity ratio of medium-to-specimen, K, and the average absolute slope of the rough surface, $\tan\theta$, are defined as follows:

$$\Theta = \frac{T - T_c}{\frac{q_m Ra}{k}}, \quad P = \frac{P_m}{\sigma_y}, \quad K = \frac{k}{k_s}, \quad \tan\theta = \frac{1}{N}\sum_{i=1}^{N}\frac{\left|Z_{i+1} - Z_i\right|}{\Delta_i} \tag{4}$$

Here, T_c is the temperature at the top surface of specimen I, q_m is the heat flux at the bottom surface of specimen II, k_s is the thermal conductivity of the specimen, σ_y is the yield stress, N is the total number of grids, and Δ_i is the horizontal interval of two grids. The dimensionless TCC can be defined as follows:

$$H_m = \frac{h_m Ra}{k} = (\Theta_{I,\text{Interface}} - \Theta_{II,\text{Interface}})^{-1} \tag{5}$$

Here, h_m is the thermal contact conductance and is defined as the ratio of the heat flux q_m to the temperature drop at the interface ($T_{I,\text{Interface}} - T_{II,\text{Interface}}$):

$$h_m = \frac{q_m}{T_{I,\text{Interface}} - T_{II,\text{Interface}}} \tag{6}$$

2.3. Computational Method

We used a network method to solve a three-dimensional heat conduction problem where an equi-peripheral grid has been developed for the cylindrical coordinate system. The grid system can be used to express reasonable contact spot distributions at the solid-solid interface. We assumed that the deformation of each asperity is fully plastic, and the change of volume due to the deformation is to be neglected. The successive over-relaxation (SOR) method is used, and the iteration is terminated when the maximum temperature difference between the successive steps becomes less than 10^{-6}. Details of the numerical method can be found in Ref. 11.

2.4. Numerical Results

Figure 3 shows the relationship between the dimensionless TCC and mean pressure at $\tan\theta=0.0227$ with k as the parameter, where $K=0$ corresponds to vacuum and $K=2.12\times10^{-4}$ to a combination of air and brass cylinder. In the figure, the experimental results are plotted with symbols Δ, which are obtained for the air and brass ($Ra=2.2\,\mu$m) combination [10] at atmospheric pressure. The numerical results with the equi-peripheral grid system, shown by a solid line, agree well with the corresponding experiments. On the other hand, the solution with the conventional equi-angular grid system shows lower values of TCC than the experiments. As shown in this figure, the TCC increases with a power of the mean pressure for all five thermal conductivity ratios. Furthermore, the TCC increases with an increase in k, because more heat flux passes through the interstitial medium with a higher thermal conductivity of the medium. This reduces the effect of contact pressure; therefore, the power of the mean pressure decreases with an increase in k.

Figure 4 shows the relationship between the TCC and the average absolute slope of the rough surface at $P=0.0186$ and at a vacuum condition $K=0$. Here, the range of abscissa $\tan\theta$ is widened beyond the normal range encountered in the case of microscale rough surfaces by considering the measurements of Yan and Komvopoulos [7]. They reported the surface roughness profile of a carbon-coated magnetic (rigid) hard disk measured with an atomic force microscope (AFM). Analyzing the power spectrum density profile of their roughness, such a nanoscale surface roughness is confirmed to be about ten times that of the mean absolute slope for a typical ground metal surface. The figure shows clearly that the TCC increases linearly with an increase in $\tan\theta$. This indicates that the TCR can be greatly reduced when the surfaces with a higher mean slope but the same roughness height are in contact for the random rough surfaces. This is

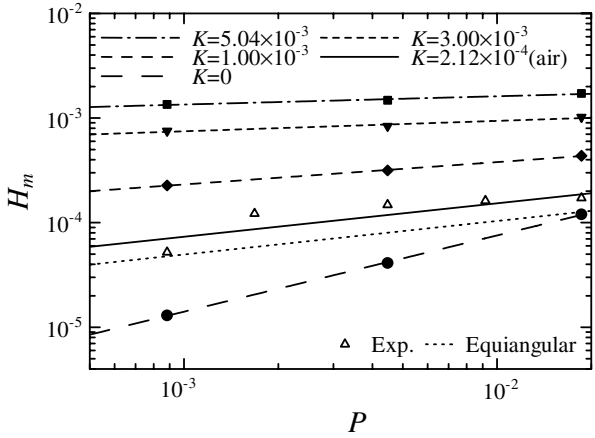

Fig. 3. Relation between contact pressure and TCC ($\tan\theta$ = 0.0227).

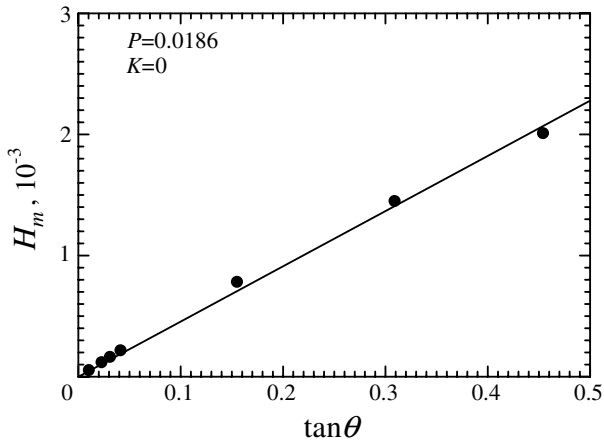

Fig. 4. Relation between average slope ($\tan\theta$) and TCC in vacuum.

attributed to the fact that the density of the contact spot, ρ_c, is greatly increased with the mean slope of roughness as shown in Fig. 5. In the figure, the contact pressure is kept constant at $P = 0.0186$; therefore, the total true contact area is not changed under the assumption of plastic deformation of asperities. The TCR is caused by the heat flow constriction at the real contact spots. Therefore, if there are more contact spots on the surface, the constriction of heat flow will be reduced, and at the same time, the TCR will be reduced.

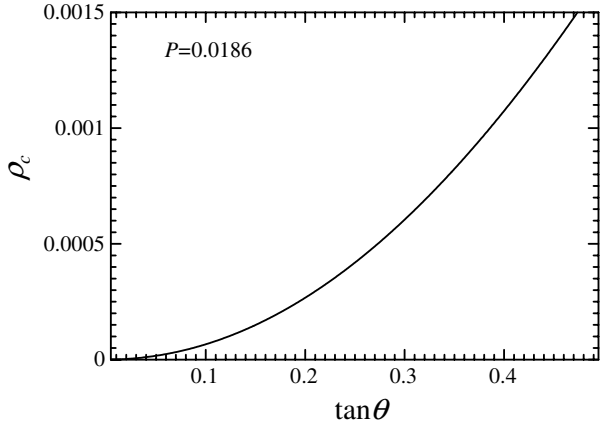

Fig. 5. Relation between average absolute slope and density of contact spots ($P = 0.0186$).

Figures 6a and 6b show the contact spot distributions at $\tan\theta = 0.02$ and 0.05, respectively. Both are obtained under the conditions of the same apparent contact area, roughness height, and contact pressure. Thus, the total true contact area of the two cases must be the same. A larger numbers of contact spots and a more uniform distribution are observed in Fig. 6b than in Fig. 6a. The temperature contours at the upper or lower contact surfaces corresponding to the above conditions are shown in Fig. 7, and isothermal lines at the cross section near the interface and the temperature profiles across the interface are shown in Figs. 8 and 9, respectively. Due to the larger numbers of contact spots and reduced heat flow constriction for $\tan\theta = 0.05$, the temperature drop at the interface is smaller than that for $\tan\theta = 0.02$. Therefore, the TCC for $\tan\theta = 0.05$ becomes higher than that for $\tan\theta = 0.02$.

3. TCC MEASUREMENTS

3.1. Experimental Setup

Figure 10 shows the experimental setup for the present measurements. A pair of brass specimens is set on a table. The heater, 5, attached to the bottom of specimen I has the same diameter as the specimens. The cooling block, 8, is mounted on the upper side of the transducer block. Ten thermocouples are inserted into the specimens along the longitudinal direction to measure the temperature distribution. The outside of the specimens is wrapped with thermal insulation to reduce heat loss. A balance machine is used to apply a load onto the specimens through the copper

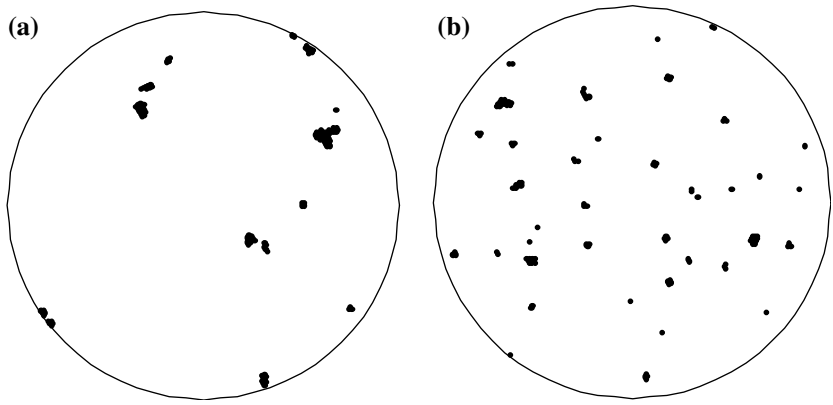

Fig. 6. Contact spot distributions ($P = 1.86 \times 10^{-2}$: (a) $\tan\theta = 0.02$ and (b) $\tan\theta = 0.05$).

block, 7. This can correctly control the load on the specimen by changing the weight without effects of thermal expansion of specimens. The ultrasonic transducer, 3, is fixed at the copper block, but it is not used in the present experiments.

A uniform heat flux was supplied at the bottom of specimen I by supplying an electrical current to the heater. A uniform and constant temperature was maintained at the top surface of specimen II by the cooling water. The temperatures of the specimens and the heating rate of the heater were measured by a system that included a scanner, two voltmeters, and a personal computer. To perform an accurate measurement, the temperature drop at the interface was maintained to be larger than 2 K, where the corresponding heating rate was about 30.0 W. The measurements were done at steady-state conditions, when the maximum temperature change over 12 min was confirmed to be less than 0.1 K.

3.2. Test Samples and Their Surface Topology

Four pairs of surface-sandblasted brass cylinders were used to measure the TCC. The cylindrical specimens have a diameter of 40 mm and a length of 45 mm. Five holes, 0.6 mm in diameter and 6 mm in depth, were drilled in each specimen to mount the thermocouples. The distance between neighboring holes is 5 mm, and the nearest one is 5 mm from the contact interface. The roughness of the brass surfaces was measured with a contact stylus profiler (SE-40c, Kozaka Lab). This instrument has a diamond stylus with a radius of 5 μm, and the relative error of longitudinal magnification is within 3%. The maximum scanning length is 30 mm,

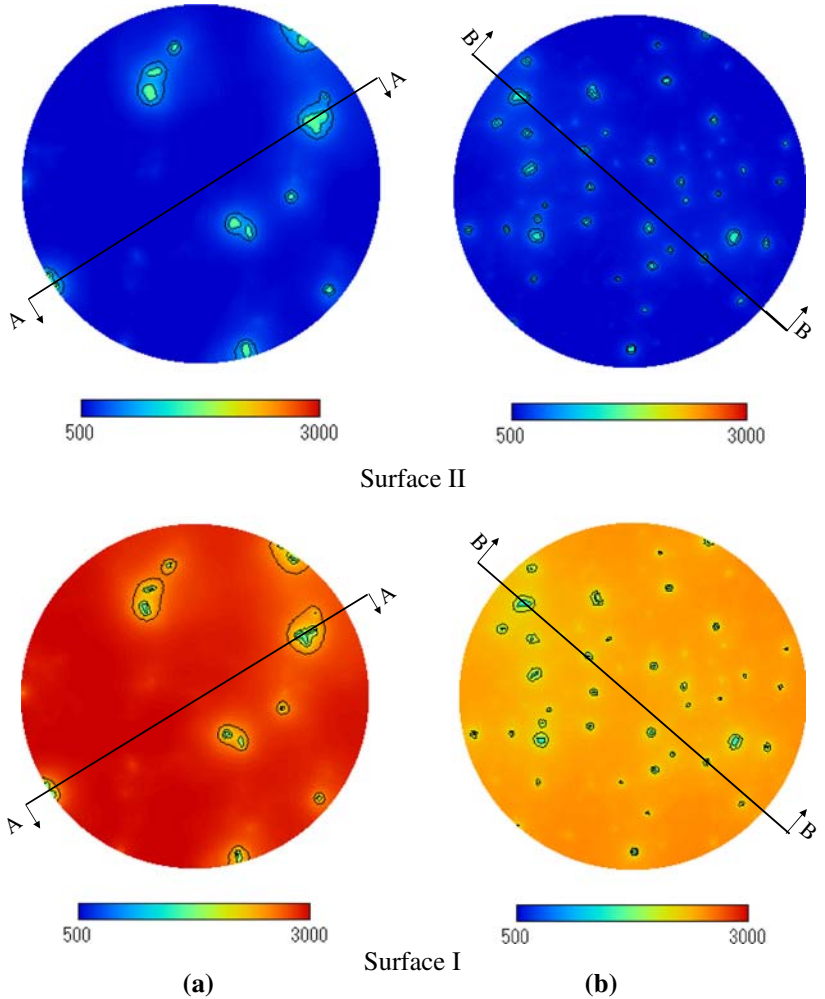

Fig. 7. Temperature distributions at the interfaces ($P = 1.86 \times 10^{-2}$: (a) $\tan\theta = 0.02$ and (b) $\tan\theta = 0.05$).

which yields 8000 evenly spaced data points. The range of the height measurement is 0.001 to 100 μm.

Two arbitrary directions of each surface were measured. Figure 11 shows the measured results of four pairs of surface roughness profiles. It is easily found that those surfaces are quite flat although the average surface roughness and average absolute slope indicated in the captions are

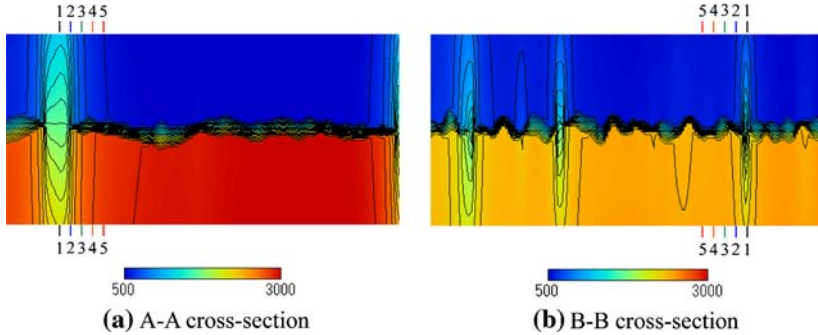

Fig. 8. Temperature distributions for cross sections ($P = 1.86 \times 10^{-2}$: (a) $\tan\theta = 0.02$ (A-A) and (b) $\tan\theta = 0.05$ (B-B)).

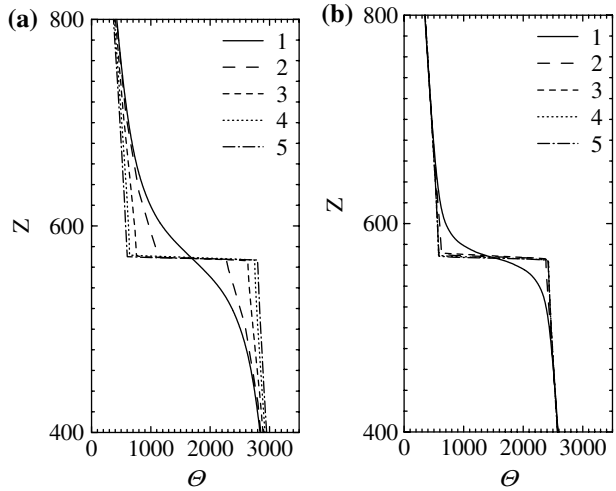

Fig. 9. Temperature distributions in Z-direction ($P = 1.86 \times 10^{-2}$: (a) $\tan\theta = 0.02$ and (b) $\tan\theta = 0.05$).

different. Pairs a, b, and c are blasted by glass beads, and pair d is blasted by grains of sand. Although the size of the glass beads used for pairs a and b is the same, Ra and $\tan\theta$ of pair b are larger than those of pair a because the processing time of pair b is longer than that of pair a. In comparing pair c with pair d, both of them have the same roughness (Ra), but the average absolute slope of pair d is 80% larger than that of pair c because the shape and material of grains are different.

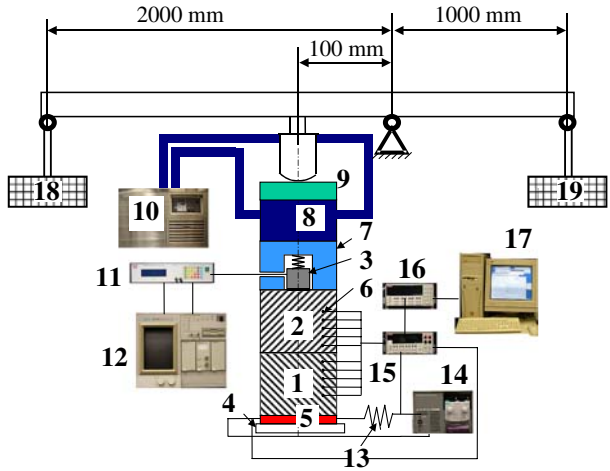

Fig. 10. Schematic diagram of experimental apparatus for TCC measurements (1 specimen I, 2 specimen II, 3 transducer, 4 acrylic board, 5 heater, 6 thermocouple, 7 copper block, 8 cooling block, 9 load cell, 10 constant temperature bath, 11 pulse receiver, 12 oscilloscope, 13 standard resistance, 14 DC power supply, 15 switch system, 16 multimeter, 17 PC, 18 weight, 19 balancing weight).

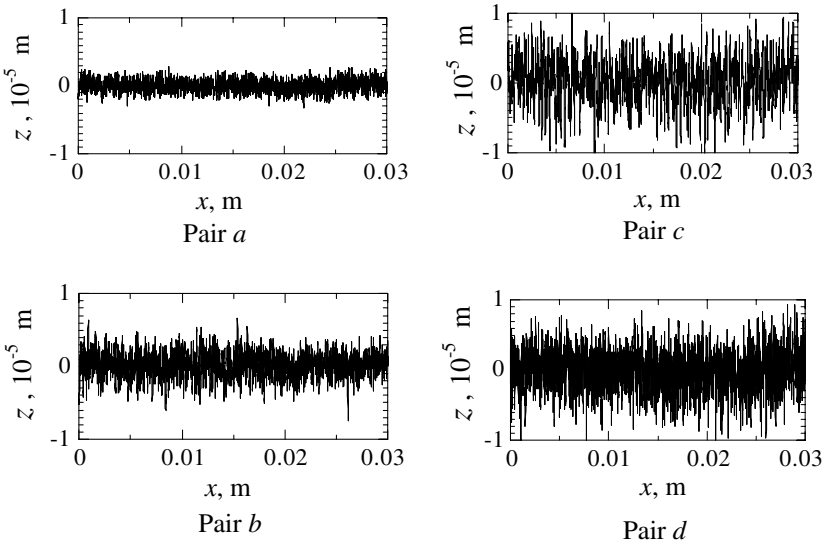

Fig. 11. Surface roughness profiles (pair a: $Ra = 0.77\,\mu$m and $\tan\theta = 0.0865$; pair b: $Ra = 1.27\,\mu$m and $\tan\theta = 0.121$, pair c: $Ra = 2.21\,\mu$m and $\tan\theta = 0.137$, and pair d: $Ra = 2.21\,\mu$m and $\tan\theta = 0.249$).

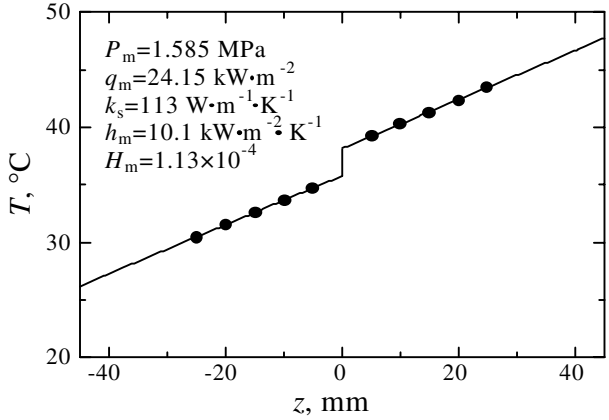

Fig. 12. Distribution of temperature in solids.

We confirmed through a statistical analysis of the surface roughness height distributions that all of these four pairs satisfy a Gaussian distribution for the roughness height. Furthermore, from an analysis of the power spectral density (PSD) of the surface roughness, it is shown that pair *d* should have a larger average absolute slope than pair *c*.

3.3. Data Processing

The temperatures at the five points of each specimen are measured and plotted in Fig. 12, as an example. Because the measurement locations are not very close to the interfaces, the temperatures in each z-plane are almost uniform. Therefore, the measured temperature can be regarded as the plane-averaged local temperature at each position. Since the temperature distribution along the z-direction is linear, the temperature gap ($\Delta T = T_{\mathrm{I}} - T_{\mathrm{II}}$) at the interfaces can be obtained from the extrapolation. On the other hand, the heat flow (Q) across the interface can be calculated from the heating rate generated by the heater. Therefore, we can obtain experimentally the TCC in dimensional and non-dimensional forms by Eqs (6) and (5), respectively.

3.4. Uncertainty Analysis

The uncertainty of the TCC measurement is considered as follows. The errors caused by the heating current, $\delta I/I$, and voltage, $\delta V/V$, are considered to be 1.4×10^{-4} and 7.6×10^{-5}, respectively. The heat loss

caused by both the bottom plate and the side thermal insulator, $\delta q_l/q_l$, is about 3.7×10^{-3}. The error caused by the diameter measurement, $\delta D/D$, is about 6.7×10^{-4}. The thermocouples inside the specimen may be located at about ±0.3 mm away from the ideal spot; this difference results in a maximum error of 6.0×10^{-2} in the temperature gradient. The maximum error of temperature measurement, $\delta T/T$, is 2.1×10^{-2}. Based on the law of error propagation

$$e_t=\sqrt{\left(\frac{\delta I}{I}\right)^2+\left(\frac{\delta V}{V}\right)^2+\left(2\frac{\delta D}{D}\right)^2+\left(\frac{\delta q_l}{q_l}\right)^2+\left(\frac{\delta \Delta l}{\Delta l}\right)^2+\left(\frac{\delta T}{T}\right)^2} \quad (7)$$

The total uncertainty of the present measurements is estimated to be $\pm6.4\%$.

4. RESULTS AND DISCUSSION

Figure 13 shows the measured results of the TCC obtained from successive loading and unloading. In the figure, pairs a, b, and c are the results of three complete loading cycles, and pair d is the result of two complete loading cycles. Also, the present numerical results corresponding to each pair of contact surfaces are indicated by a solid line. The numerical results are found to be in good agreement with the measurements. In all of the figures the first loading cycle has a different path. It means that most of the plastic deformation of asperities occurs in the first loading cycle. For the first unloading path, the asperities have already been flattened plastically after the first loading to the highest pressure so that the true contact area and TCC increase relatively at the corresponding load. Since the load was not removed completely from the specimens at the beginning of the second and third cycles, the relative position of each specimen was not changed. However, a small amount of plastic deformation is still observed from the hysteresis exhibited by the cycles. Although pair c and pair d have the same surface roughness ($Ra=2.21\,\mu$m), the measured TCC of pair d is larger than that of pair c because they have different $\tan\theta$ ($c:\tan\theta=0.137$, $d:\tan\theta=0.249$). This result clearly confirms the numerical prediction that the TCC increases with an increase in $\tan\theta$ for the same mean surface roughness. To demonstrate the effect of the average absolute slope of the surface roughness, the relation between the average absolute slope, $\tan\theta$, and the dimensionless TCC, H_{m}, at a constant pressure ($P=0.0057$, $P_m=1.68$ MPa) is shown in Fig. 14. The TCC, H_{m}, is proportional to the average absolute slope, $\tan\theta$. Also, the present experimental results agree well with the numerical predictions, although the latter gives a little higher values than the former.

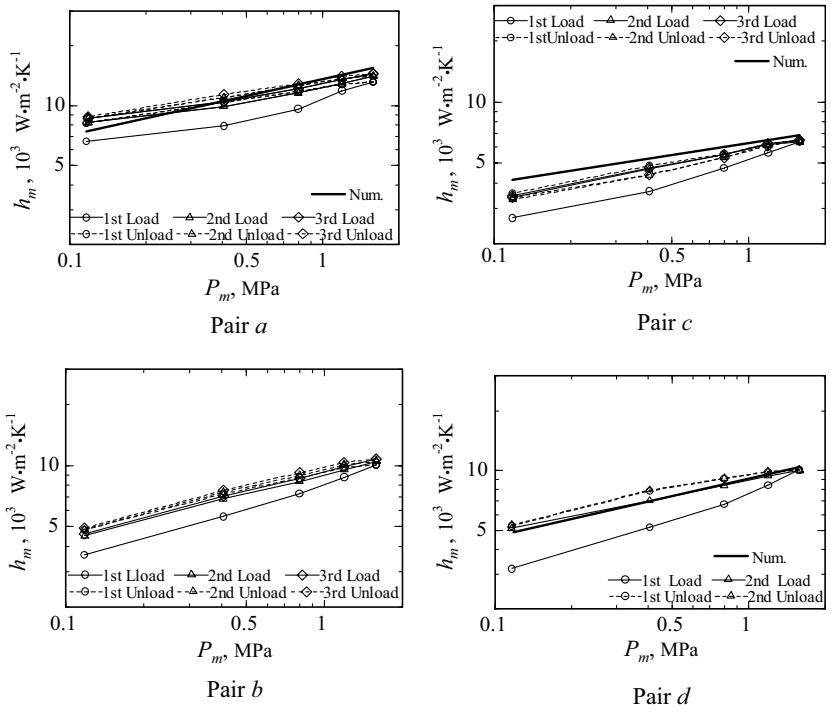

Fig. 13. Relation between contact pressure and TCC.

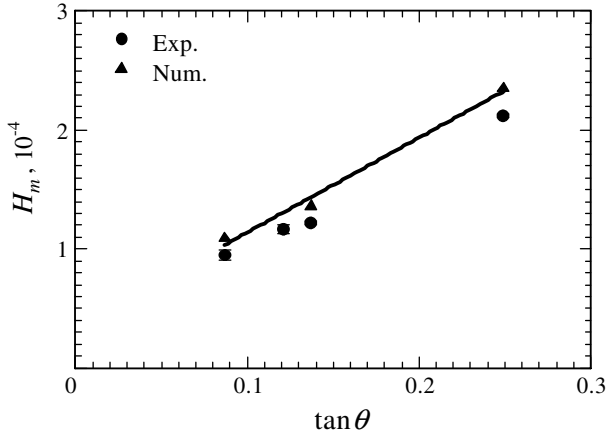

Fig. 14. Relation between average absolute slope and TCC with contact pressure ($P = 0.0057$).

5. CONCLUSIONS

Numerical simulations and experiments of the TCC at the interfaces of two cylinders in contact have been carried out for various surface configurations and contact pressures. Numerical results show that the dimensionless TCC increases with an increase in the mean pressure, in the thermal conductivity ratio of medium-to-specimen, and in the average absolute slope of the rough surface. The hysteretic nature of the contact pressure on TCC was observed experimentally between the first and second loading cycles. The experimental results agree with the numerical predictions that the dimensionless TCC increases with an increase in the mean absolute slope of surface roughness at a constant contact pressure and average surface roughness. The present results demonstrate a new way to reduce the thermal contact resistance in practical engineering applications.

NOMENCLATURE

B	dimensionless scale factor
D	diameter of specimen (m)
H_m	dimensionless thermal contact conductance
h_m	thermal contact conductance ($W \cdot m^{-2} \cdot K^{-1}$)
I	heating current (A)
K	thermal conductivity ratio of medium-to-specimen
k	thermal conductivity of specimen ($W \cdot m^{-1} \cdot K^{-1}$)
L	length of specimen (m)
L_i	dimensionless wavelength of surface roughness
l_i	wavelength of surface roughness (m)
N	total number of grids
n	upper limit number of superposed waves
P	dimensionless mean nominal contact pressure
P_m	mean nominal contact pressure (Pa)
q_m	heat flux ($W \cdot m^{-2}$)
R	dimensionless radius in cylindrical coordinates
r	radius in cylindrical coordinates (m)
R_0	dimensionless radius of specimen
R_a	mean roughness (m)
RND	random number
$R_{\max}$	maximum roughness (m)
T	temperature (K)
T_c	temperature at the top surface (K)
V	voltage (V)
Z	dimensionless axis in cylindrical coordinates

z	axis in cylindrical coordinates (m)
$Z(R, \theta)$	dimensionless height of surface roughness
α_i	orientation
Δ_ι	horizontal interval of two grids
Θ	dimensionless temperature
θ	angle in cylindrical coordinates
σ_y	yield stress (Pa)
ρ_c	density of the contact spots

Subscripts

I	specimen I
II	specimen II
i	number
min	minimum
max	maximum

REFERENCES

1. V. Sartre and M. Lallemand, *Appl. Therm. Eng.* **21:**221 (2001).
2. H. Fenech and W. M. Rohsenow, *Trans. ASME, J. Heat Transfer* **8:**15 (1963).
3. M. G. Cooper, B. B. Mikic, and M. M. Yovanovich, *Int. J. Heat Mass Transfer* **12:**279 (1969).
4. B. B. Mikic, *Int. J. Heat Mass Transfer* **17:**205 (1974).
5. K. L. Johnson, *Contact Mechanics* (Cambridge University Press, Cambridge, England, 1985).
6. A. Majumdar and C. L. Tien, *Trans. ASME, J. Heat Transfer* **113:**516 (1991).
7. W. Yan and K. Komvopoulos, *J. Appl. Phys.* **84:**3617 (1998).
8. R. V. Francois, *Wear* **249:**401 (2001).
9. M. Bahrami, J. R. Culham, M. M. Yovanovich, and G. E. Schncider, *Proc. ASME Heat Transfer Conference*, Las Vegas (2003), Paper No. HT2003–47051.
10. T. Tomimura, Y. Matsuda, X. Zhang, and M. Fujii, *JSME Int. J.* **43**:665 (2000).
11. X. Zhang, P. Z. Cong, S. Fujiwara, and M. Fujii, *Int. J. Heat Mass Transfer* **47:**1091 (2004).